



Screening of Anti-cancer Activity of rGO–Bi₂O₃ Nanocomposite on Apoptosis in A549 and NCI-H460 Lung Cancer Cell Lines

S. Arockia Anushya¹ · S. Prabhu² · Vilwanathan Ravikumar² · A. Philominal¹

Received: 24 August 2022 / Accepted: 23 February 2023 / Published online: 16 March 2023
© The Author(s), under exclusive licence to Springer Science+Business Media, LLC, part of Springer Nature 2023

Abstract

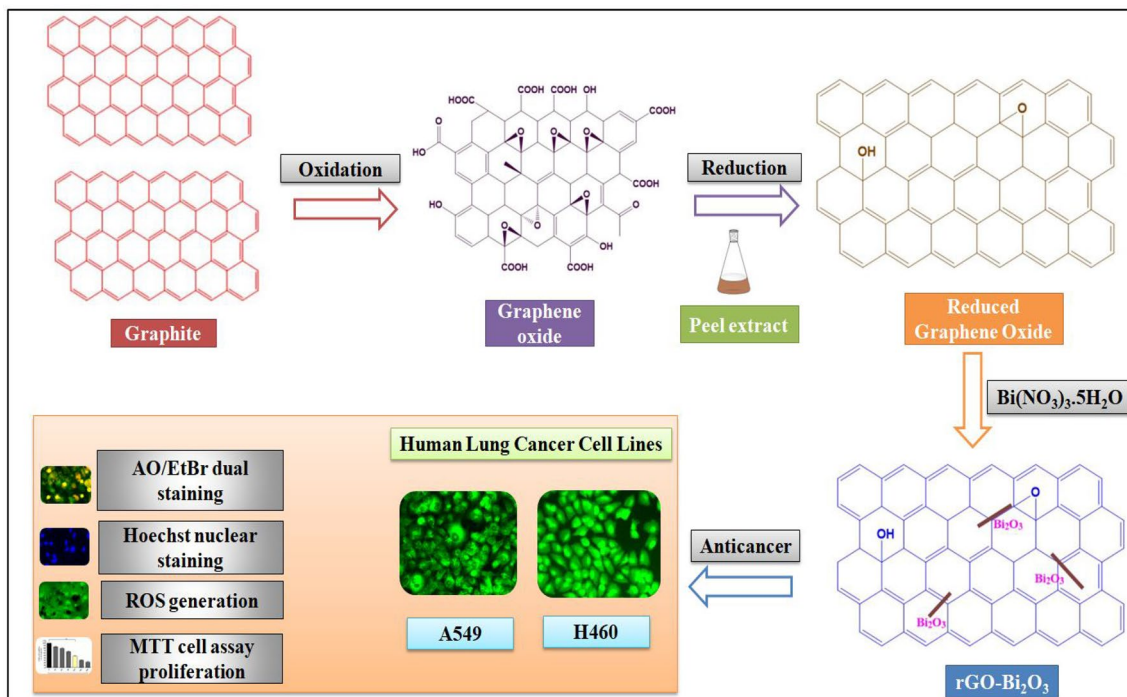
The present study emphasizes the inclusion of bismuth oxide (Bi₂O₃) with reduced graphene oxide (rGO) enhances the anti-cancer properties leading us to investigate cytotoxicity and apoptosis on lung cancer cell lines. Non-small cell lung cancer A549 and NCI-H460 were treated with graphene oxide (GO), rGO, and rGO–Bi₂O₃ nanocomposite, successfully prepared using the hydrothermal method by adopting green reduction of GO. The synthesized materials were confirmed by various characterizations such as X-ray diffraction, FT-Raman spectroscopy, Scanning electron microscopy, Energy dispersive X-ray analysis, and Fourier transform infrared spectroscopy. The interlayer is observed to be reduced for rGO as compared to that of GO because of the removal of oxygen functional groups, whereas the d-spacing for rGO–Bi₂O₃ nanocomposite is almost the same as for rGO. Raman excitation peaks were obtained by a laser wavelength of 532 nm. The increase in the intensity of D and G bands (ID/IG) for rGO is due to implying restoration of the p-conjugation increase in order by reduction. SEM shows the growth of Bi₂O₃ nanoneedles on the rGO sheets, and nanocomposite-containing elements such as carbon, oxygen, and bismuth were certain by EDAX. The functional groups were examined using the intensity of FTIR peaks. Zeta potential analysis, negative value of –3.86 mV was identified for rGO–Bi₂O₃ nanocomposite. The half maximal inhibitory concentration (IC₅₀) was found to be 160 µg/mL and 150 µg/mL for GO, 150 µg/mL and 120 µg/mL for rGO, and 60 µg/mL and 80 µg/mL for rGO–Bi₂O₃ nanocomposite. It is expected that this investigation would be useful to develop GO, rGO, and rGO–Bi₂O₃ nanocomposite-based anticancer activity to detect its effects on apoptosis in cancer cells.

✉ A. Philominal
filoje@gmail.com

¹ PG and Research Department of Physics, Holy Cross College (Autonomous), Affiliated to Bharathidasan University, Tiruchirappalli, Tamil Nadu 620 002, India

² Department of Biochemistry, School of Life Science, Bharathidasan University, Tiruchirappalli, Tamil Nadu 620 024, India

Graphical Abstract



Keywords Reduced graphene oxide · Bismuth oxide · Hydrothermal · Cytotoxicity · Non-small cell lung cancer

1 Introduction

Lung cancer is a devastating disease that affects both men and women, and it is the second most common cause of cancer death in humans. Lung cancer accounts for 18.4% of all cancer-related deaths. Only 15% of people with lung cancer survive following diagnosis. However, around 70% of cases are in a progressive state at the time of diagnosis. The majority of women suffered due to significant reasons mortality from the consequences of cancer [1, 2]. Small cell lung cancer (SCLC) and non-small cell lung cancer (NSCLC) are two basic forms of lung cancer. Many attempts were made to treat lung cancer with various methods such as radiation therapy, chemotherapy, and various medications. These methods are not effective due to damaging healthy tissue and non-targeted [3]. To overcome this, specific features of nanomaterials increased their application in medical science as a novel carrier for cancer therapy. Among them, carbon nanomaterials have unique physicochemical properties and have been widely used in the field of nanomedicine [4, 5]. Nevertheless, there is intense attention to carbon. Since 2004, Graphene has emerged as a rising star in carbon nanomaterials [6, 7]. A planar monolayer of sp²-bonded carbon atoms in a single sheet of graphene is arranged on a two-dimensional honeycomb lattice, which is made of hexagonal rings [8].

Graphene oxide (GO), an oxidized version of the graphene material, has a sustained density of functional groups like carbonyl, epoxy, carboxyl, and hydroxyl groups. [9]. The reduction of GO under pressure and temperature is monotonous, costly, and has potential dangers for the environment. Thus, it's required to have non-dangerous, minimal effort, and non-lethal strategies. One of the strategies to produce reduced GO in an eco-friendly way is achieved by green reduction, which has expanded nowadays [10].

Pomegranate is a fruit of two species comprising the punicaceae family. Among juice, peel, and seed, the peels possess a higher content of polyphenols. This part of the fruit contains a large number of polyphenols with a molecular weight greater than 1000, which include minor ellagic and gallic acids [11]. Due to the ability to donate hydrogen atoms or electrons easily, polyphenols are regarded as effective reducing agents. The reductive property of polyphenol has enabled the production of single-wall carbon nanotubes well-dispersed in water and its use in the synthesis of metal nanoparticles [12]. The oxygen functions may be eliminated during the reduction process, which significantly improves the optical surface characteristics and modifies the electronic structure [13]. In recent times, graphene sheets decorated with metal oxide nanocomposites have captured significant attention due to their unique properties and synergetic effect

between them, leading to a large variety of applications. To date, the most important metal oxide nanoparticles supported on graphene, include ZnO [14], MnO₂ [15], TiO₂ [16], Fe₃O₄ [17], SnO₂ [18], and Cu₂O [19]. The addition of Bi₂O₃ to any material enhances the chemical and physical properties of the material. The inclusion of such nanomaterials in the carbon-based material prevents oxidation and aggregation. It is advised to prepare rGO–Bi₂O₃, which has potent anticancer properties and negligible adverse effects on both humans and the environment [20]. The non-toxic nature of Bi₂O₃ is significant to work in anticancer activity against human cancer cell lines [21, 22].

Numerous studies have recently examined the *in vivo* and *in vitro* toxicity of graphene. However, the harm caused by this substance is still unclear because both nontoxic and toxic effects were observed. These disparities could be due to variations in physicochemical characteristics, such as lateral dimensions, chemical composition, surface area, purity, morphology, functional groups, coatings, charges, dissolving media, etc. Studies have shown that graphene-based nanomaterials are benign and nontoxic for use in biological applications. The mechanism utilized to explain the cytotoxic effect is what generates the oxidative stress produced by reactive oxygen species (ROS) [23]. Graphene is the latest membrane, to improve our knowledge on the subject of the molecular mechanism underlying graphene-induced toxicity, and explicate the role of A549 and NCI-H460 cells when exposed to GO, rGO, and rGO–Bi₂O₃ nanocomposite. As an *in vitro* model, there have been multitudes of studies on non-toxicity carried out using A549 and NCI-H460 cell lines. A549 and NCI-H460 is not the only conventional model to study lung cancer responses but also a vast number of experiments that can be done in a short duration of time by their relative ease of culture [24].

The novelty aspect of this work is that the cytotoxicity and apoptotic potential of GO, rGO, rGO–Bi₂O₃ nanocomposite in A549 and NCI-H460 lung cancer cell lines is reported for the first time, to the best of our knowledge. Though there are many literature reports available for understanding the effects of rGO–Bi₂O₃ nanocomposite on magnetic and catalytic properties [25–28]. However, there is no conglomeration of rGO–Bi₂O₃ nanocomposite exposure on A549 and NCI-H460 cells. In the past few decades, a lot of nanomaterials were used against lung cancer cell lines identified and reported in the literature [5, 29–33]. The rapid development of nanodrug formulation for anticancer activity proposes a serious challenge to identifying a nanomaterial that shows a promising anticancer capability.

Therefore, in this article, it is aimed to develop an inexpensive, eco-friendly, and simple method to synthesize rGO using pomegranate peel extract, which was then tested for the presence of phytochemicals. The effects of the rGO–Bi₂O₃ nanocomposite developed from the

hydrothermal method were optimized, followed by the calcination behavior at 300 °C. Further, the effectiveness of GO, rGO, and rGO–Bi₂O₃ nanocomposite against lung cancer cells A549 and NCI-H460 was also studied. Cytotoxicity and apoptosis were used to investigate a potential anticancer mechanism. These cell lines were selected in the present study because A549 and NCI-H460 are known as NSCLC which is the leading cause of cancer, where 84% of lung cancer is NSCLC which is much higher than that of the SCLC (13%).

2 Materials and Methods

2.1 Materials

Graphite flakes (-325 mesh, purity 99.8%) were obtained from alfa aesar, India. Sodium nitrate (NaNO₃, 99%), potassium permanganate (KMnO₄, 98.5%), concentrated sulfuric acid (H₂SO₄, 97%), hydrogen peroxide (H₂O₂, 30%), bismuth nitrate pentahydrate (Bi(NO₃)₃·5H₂O, 98.5%), hydrochloric acid (HCl), hydrazine hydrate (80%), Ammonia solution (30%) were purchased from Merck, India and are used without further purification.

2.2 Synthesis of GO by Modified Hummer's Method

2 g of graphite flakes and 1 g of NaNO₃ were mixed with 46 mL of Con.H₂SO₄ and stirred for an hour in an ice bath. 6 g of KMnO₄ were divided into three parts and added at a 30 min interval at < 10 °C. Subsequently, the prepared solution was allowed to stir for 1 h at 35 °C after the removal of an ice bath. The solution was diluted by adding 150 mL of double-distilled (DD) water under vigorous stirring for an hour. The resulting solution was kept in the reflux system at 95 °C for 30 min. Thereafter, the solution was further diluted by adding 100 mL of DD water and, stirring continued for 1 h. Subsequently, 30% H₂O₂ was added dropwise until the color of the solution turn into yellow. The resulting material was washed with HCl and DD water until the pH became neutral with the assistance of ultrasonication and centrifugation. The final product was dried for 24 h at 60 °C [34].

2.3 Preparation of Pomegranate Peel Extract

A certain amount of pomegranate peel was cut into small pieces and dried for several days. The dried peels were powdered, and 10 g of powdered peel were dispersed into 100 mL of DD water and exposed to heat for an hour at 80 °C with constant stirring. A light brown colored extract was then filtered and stored at – 4 °C for further purposes.

2.3.1 Phytochemical Analysis

Phytochemical analysis of pomegranate peel extract was carried out by the standard method to identify the primary and secondary metabolites driven by Yadav [35].

2.3.2 Test for Phenols

0.5 g of dried peel extract was dispersed in 20 mL of DD water and heated at 50 °C for 30 min. The peel extract was collected by filtration and 2 mL of plant extract was taken, followed by the addition of ammonia solution. The color of the solution turns reddish-orange which indicates the presence of phenol.

2.3.3 Determination of Total Phenolic Content

0.5 g of peel was extracted with 2 mL of DD water and incubated for 5 min at room temperature. A few drops of ammonia and amyl chloride were added to the above solution. The supernatant was allowed to evaporate to dryness.

2.4 Synthesis of Reduced Graphene Oxide

100 mg of GO was mixed in 200 mL of DD water and was ultrasonicated for 30 min. 10 mL of pomegranate peel extract was added under stirring for 6 h. Followed by refluxing the final solution for 6 h in a water bath. The product was ultrasonicated and centrifuged, then washed with DD water until a clear solution is obtained. The resulting product was dried for 24 h at 60 °C by using a hot air oven.

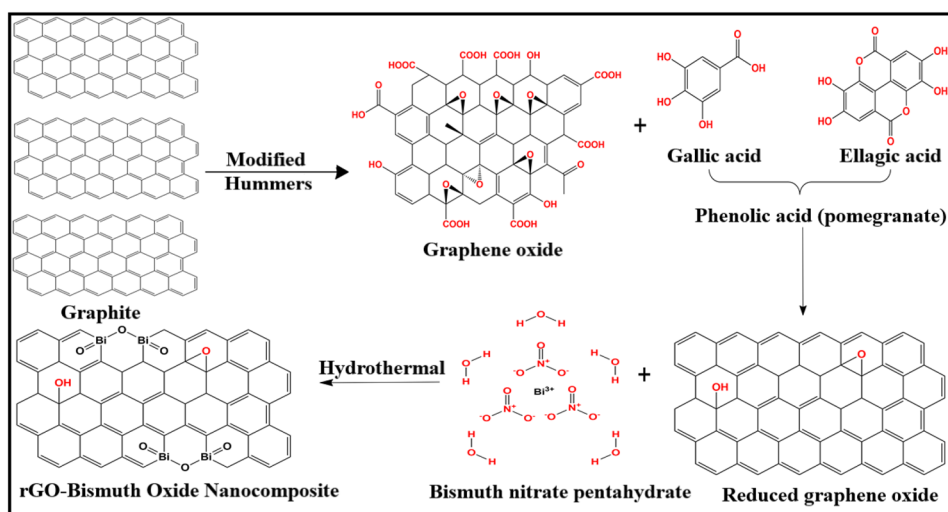
2.5 Controlled Experiment

A controlled experiment was carried out in DD water to ensure the reduction of graphene oxide by pomegranate peel extract. The GO (0.5 mg/mL) dispersion was refluxed at 95 °C for 8 h. The color of the GO dispersion (DGO) remains unchanged compared to the aqueous dispersion of pure GO. This experiment confirmed that the pomegranate peel extract plays a vital role in the reduction of GO. Another experiment was carried out using Hydrazine to compare the quality of rGO to Hydrazine-reduced Graphene Oxide (HR-GO). For this, 0.5 mL of hydrazine hydrate was added to 100 mL GO (0.5 mg/mL) dispersion and was refluxed at 95 °C for 8 h [36]. The preparation of rGO-based nanocomposite is summarised within Fig. 1 and Fig. 2 shows the differently prepared samples to confirm the reduction of GO by pomegranate peel extract.



Fig. 2 Digital photograph of GO, rGO, HR-GO, and DGO. GO graphene oxide, rGO reduced graphene oxide, HR-GO hydrazine reduced graphene oxide, DGO distilled water reduced graphene oxide

Fig. 1 Schematic illustration for the formation of the rGO–Bi₂O₃ nanocomposite



2.6 Preparation of rGO–Bismuth Oxide Nanocomposite

rGO–Bi₂O₃ nanocomposite with an equimolar ratio was prepared by dispersing 10 mg of rGO in 90 mL of DD water. A certain amount of Bi(NO₃)₃·5H₂O was added to 5 mL of HNO₃ and 25 mL of water. Both the suspension was subjected to 1 h sonication. The Bi solution was added to the above reaction mixture under vigorous stirring for 20 min at 150 °C. Ammonia solution was added dropwise to make the pH 9. The final precipitate was taken without washing and transferred to an autoclave (containing 20 mL of DD water). The autoclave was heated in a hot air oven at 180 °C for 12 h. The obtained product was ultra-sonicated, centrifuge washed, and dried at 100 °C for 12 h. The dried product was further heated at 300 °C for 2 h.

3 Characterization

X-ray diffraction (XRD) pattern was analyzed by (Model PANalytical/X Pert3 powder) in the range of 5–80 °C for the analysis of crystalline size and composition. LabRAM HR Evolution Raman spectrometer was used to analyze the microstructure of samples with the wavelength of a 532 nm laser beam. The surface morphology was recorded by Carl Zeiss Scanning electron microscope (SEM). The elemental composition analysis was done by Energy Dispersive X-ray Analysis (EDAX) (AMETEK). Fourier-transform infrared (FT-IR) spectra of GO, rGO, and rGO–Bi₂O₃ were carried out in the range of 4000–400 cm⁻¹ using a Perkin Elmer Frontier FT-IR spectrometer. The stability of the rGO–Bi₂O₃ nanocomposite was carried out by zeta potential analyzer by Malvern Instrument.

3.1 Cancer Cell Maintenance

Two human lung cancer cell lines A549 and NCI-H460 were purchased from the National Centre for Cell Science, Pune, India. Cells were cultured in complete Dulbecco's Modified Eagle's Medium (DMEM) containing 1% (v/v) penicillin–streptomycin antibiotic solution (Hi-Media Laboratories, Mumbai, India) and 10% (v/v) Fetal Bovine Serum (FBS) (Thermo Fisher Scientific, USA). Cells were maintained in the presence of 37 °C and 5% humid atmosphere CO₂.

3.2 MTT Cell Proliferation Assay in A549 and NCI-H460

The concentration range of GO, rGO, and rGO–Bi₂O₃ nanocomposite was 20–180 µg/mL. Briefly, the cells were cultured at a density of 1 × 10⁴ per well and were grown in 96 well plates and incubated overnight with 5% CO₂ at 37 °C.

The cells were incubated with different concentrations of GO, rGO, and rGO–Bi₂O₃ for 24 h. Further, 20 µL of MTT (5 mg/1 mL 1 × PBS) solution was added to every well and incubated for 4 h. MTT was aspirated and 100 µL of DMSO was added to each well to solubilize the formazan crystals. The optical density was calculated at 595 nm using a multi-well plate reader (Bio-Rad, USA). All the mentioned procedures were performed in triplicate and the percentage of viability was calculated using the formula:

$$\% \text{ of Viability} = \frac{\text{Optical Density value of Experimental Sample}}{\text{Optical Density value of Experimental Control}} \times 100 \quad (1)$$

3.3 Apoptotic Studies by Fluorescent Staining

The effects of GO, rGO, and rGO–Bi₂O₃ on A549 and NCI-H460 cells apoptosis were determined morphologically using a fluorescent microscope (Fluoid cell imaging station), after labeling with acridine orange and ethidium bromide (AO/EtBr). In brief, both types of lung cancer cell lines were cultured at 5 × 10⁵ cells/well in 6-well plates and treated with a lethal dose (IC₅₀) of GO, rGO, and rGO–Bi₂O₃ nanocomposite and incubated for 24 h. Further, cells were stained with AO/EtBr (1:1 v/v from 100 µg/mL in PBS) and images were captured using a fluorescent microscope.

3.4 ROS Generation—DCFH-DA Assay

The fluorescent marker 2', 7'-dichlorofluorescein-diacetate (DCFH-DA) was used to measure the intracellular generation of reactive oxygen species (ROS). NSCLC cell lines were seeded in 6-well plates and maintained in 5% CO₂ and 95% humidified conditions. After 60–80% confluency cells were treated with GO, rGO, and rGO–Bi₂O₃ nanocomposite and incubated for 24 h. Further, the culture plate was incubated with 40 µM of DCFH-DA in 1 × PBS for 30 min and washed once in 1 × PBS. The images of cells were captured using a 20 × objective fluorescence microscope.

3.5 Hoechst Nuclear Staining

To capture apoptotic induction of GO, rGO, and rGO–Bi₂O₃ nanocomposite in A549 and NCI-H460 cell nucleus Hoechst 33,258 staining was performed. Cells were cultured at a density of 1 × 10⁵/well mL in a 6-well plate and incubated for 24 h. Followed by, the cells were stained with 50 µL/mL of Hoechst 33,258 and incubated for 30 min. The changes in the nuclei of the cell were captured using a 20 × objective fluorescence microscope.

3.6 Statistical Analysis

The grouped data were statistically analyzed using GRAPH-PAD PRISM 4 to detect the statistical significance. The values were expressed as average \pm standard deviation (SD). The data was statistically significant when $p \leq 0.05$.

4 Results and Discussion

4.1 Estimation of Total Phenols

Phytochemical analysis of pomegranate peel extract supplies fundamental information about the primary and secondary metabolites present in the aqueous peel extract. The peel parts of pomegranate contain a large number of polyphenols, gallic acid, ellagic acid, and tannins. The preliminary Phyto constituent analysis of pomegranate peel extract displays the presence of saponins, tannins, flavonoids, alkaloids, steroids, proteins, carbohydrates, and phenols (Table 1).

Upon quantification, the total phenolic content in pomegranate peel extract was found to be higher when compared with the other metabolites 2.5% in 0.5 g of plant sample.

4.2 X-ray Diffraction (XRD)

The XRD pattern of pure GO, rGO, and rGO–Bi₂O₃ are shown in Fig. 3 The XRD reflection peak of GO centered at 11.09° (002) corresponds to a d-spacing of 8.5 Å. The larger d-spacing is due to the formation of hydroxyl, carboxyl, and epoxy (oxygen functional groups) and allowing the water molecules to intercalate between layers in graphite. The peak was shifted from 11.09° of GO to 24.79° rGO corresponding to an interlayer spacing of 3.7 Å which is lower than that

Table 1 Preliminary phytochemical screening of pomegranate peel extract of selected samples

Phyto constituents	Conclusion
Saponins	++
Tannins	+
Flavonoids	+++
Alkaloids	++
Steroids	++
Proteins	+
Quinones	–
Glycosides	–
Resins	–
Carbohydrates	++
Phenols	+++

– not present, + present in small concentration, ++ present in moderately high concentration, +++ present in high concentration

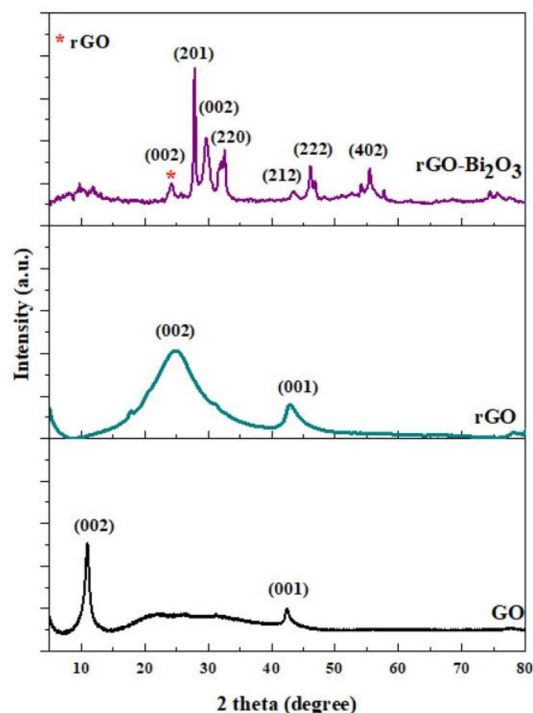


Fig. 3 Powder XRD patterns of GO, rGO, and rGO–Bi₂O₃ nanocomposite

of the GO. This observation indicates that there is an exfoliation of absorbed water molecules and oxygen functional groups during the green reduction process which indicated reinstatement of the sp² network on reduction. An increase in the oxygen content in the composite, in addition to Bi₂O₃ NPs. The diffraction plane (002), (201), (002), (220), (212), (222), (402), and (423) corresponds to the JCPDS file (78-1793) of Bi₂O₃. The d-spacing of 3.6 Å, 3.2 Å, 2.8 Å, 2.7 Å, 2.0 Å, 1.9 Å, 1.6 Å, 1.2 Å corresponds to the diffraction plane respectively.

4.3 FT-Raman Spectroscopy

Raman scattering is useful to characterize graphene materials because of its strong dependency on the electronic structure. Figure 4 shows the Raman spectra of GO, rGO, HR-GO, and rGO–Bi₂O₃. Two main features are generally characterized in the Raman spectra of graphene: The G band is generally observed at 1575 cm⁻¹ arising from the first-order scattering of E_{2g} phonons by sp² carbon atoms and the D band is observed at 1350 cm⁻¹ due to a breathing mode of j-point photons of A_{1g} symmetry. For GO, the G band shifted to 1593 cm⁻¹, and the D band shifted to 1346 cm⁻¹. The intensity ratio (ID/IG) of GO was found to be 0.86. Interestingly, the G and D bands of rGO are observed at 1588 cm⁻¹ and 1346 cm⁻¹ with the intensity ratio (ID/IG) found to be 1.00 which is higher than that of GO. To compare the

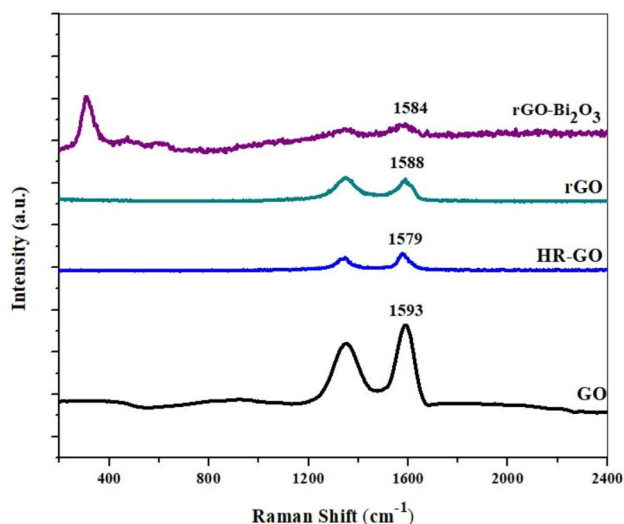


Fig. 4 Comparison between FT-Raman spectra of GO, rGO, HR-GO, and rGO–Bi₂O₃ nanocomposite

quality of green reduction with chemical reduction, rGO (pomegranate reduction) is compared with HR-GO (hydrazine reduction) indicating the successful reduction. It can be seen that the (ID/IG) ratio of HR-GO is 0.98 which is almost similar to rGO, indicating the reduction of GO by pomegranate peel extract is comparable to that of hydrazine. For the as-prepared nanocomposite, the presence of Bi–O bands was observed at 307 cm⁻¹ and 467 cm⁻¹ whereas the G band and D band are found to be at 1584 cm⁻¹ and 1346 cm⁻¹ with an intensity (ID/IG) ratio of 0.99. This observation indicates the reduction of GO to rGO and the formation of rGO–Bi₂O₃ [37].

4.4 Scanning Electron Microscopy (SEM)

The surface morphology and particle size of the prepared material were analyzed by SEM. In Fig. 5a surface morphology of GO is observed as a wrinkled surface with multiple layers. This was due to the oxygen functional group present on the surface of the GO sheets. Figure 5b exhibits stacked wrinkled-like rGO confirming the formation of a 2D structure that indicates graphene oxide has been reduced during the green reduction process. The needle-shaped nanocrystals confirm the successfully grown Bi₂O₃ on the surface of graphene nanosheets (Fig. 5c, d).

4.5 Energy Dispersive X-ray Analysis (EDAX)

The elemental compositions of rGO–Bi₂O₃ nanocomposite were carried out through EDAX techniques. The EDAX spectrum of rGO–Bi₂O₃ nanocomposite shows the presence of carbon, oxygen, and bismuth elements with an atomic percentage of 55.74%, 37.24%, and 7.02% respectively

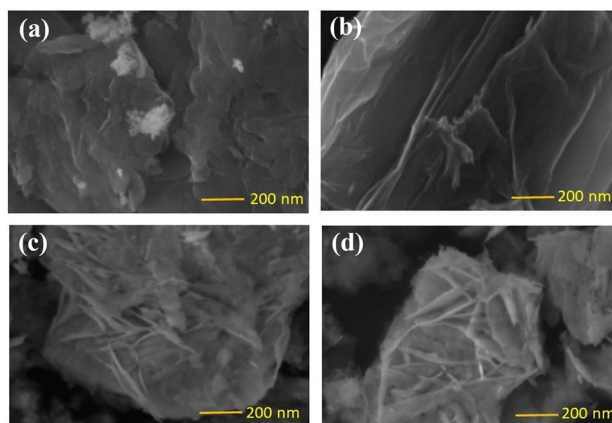


Fig. 5 Scanning electron microscopy of synthesized samples. **a** SEM analysis of GO, **b** SEM analysis of rGO, and **c–d** SEM analysis of rGO–Bi₂O₃ nanocomposite

(Fig. 6). The elemental composition analysis of rGO–Bi₂O₃ nanocomposite has confirmed the presence of Bi₂O₃ on rGO sheets.

4.6 FT-IR Spectroscopy

Figure 7 shows the functional moieties present in GO, rGO, and rGO–Bi₂O₃ nanocomposite. The strong intense absorption peak at 3420 cm⁻¹ of GO sample related to OH stretching associated with either hydroxyl group which is a sign of the presence of oxygen-containing moieties like carboxylic, carbonyl, hydroxyl, and epoxy in GO or water molecules absorbed by GO. CH₂ groups are to be found at 2925 cm⁻¹ and 2855 cm⁻¹ which are associated with symmetric and asymmetric vibrations. The peak observed at 1723 cm⁻¹ is related to C=O (carbonyl group) which indicates the occurrence of oxidation. Peaks associated with hydroxyl deformation are seen at 1624 cm⁻¹ (O–H stretching vibrations), and epoxy stretching at 1383 cm⁻¹ (C–O stretching vibrations).

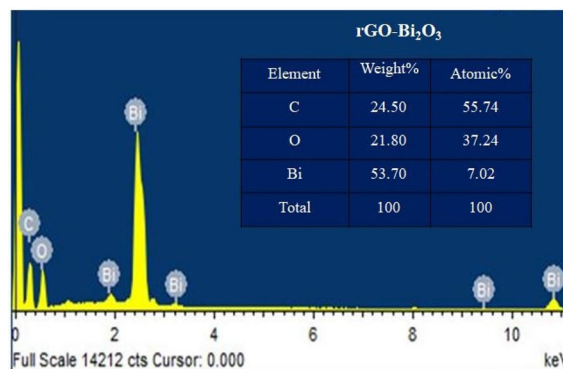


Fig. 6 Energy dispersive X-ray analysis of synthesized rGO–Bi₂O₃ nanocomposite

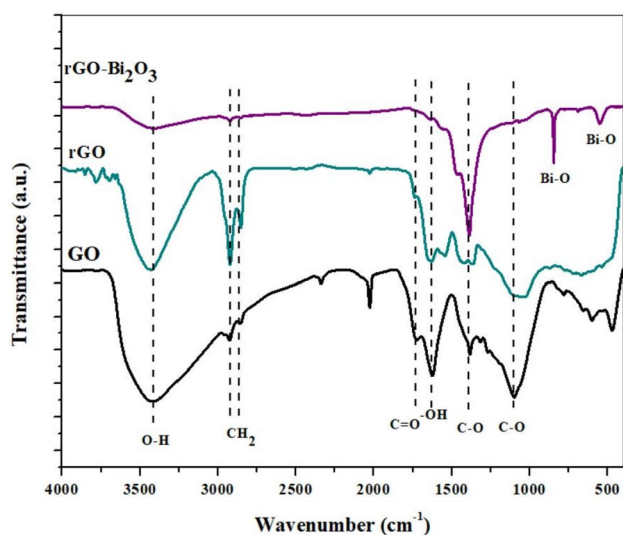


Fig. 7 FTIR analysis of GO, rGO, and rGO-Bi₂O₃ nanocomposite

For rGO, the presence of an intense peak at 2922 cm⁻¹ and 2853 cm⁻¹ than GO is due to the β-carotene absorption of the graphene surface. Very weak peaks at 1629 cm⁻¹, 1363 cm⁻¹, and 1095 cm⁻¹ indicate the amount of carbonyl, carboxyl, and epoxy groups are reduced than that in GO. Thus, resulting in the oxygen-containing groups were successfully eliminated in rGO samples. For rGO-Bi₂O₃ spectra display broad peaks at 845 cm⁻¹, 690 cm⁻¹ and 552 cm⁻¹ confirming the successful preparation of Bi-O NPs which corresponds to metal oxide (M-O stretching vibrations). The intense peak at 1385 cm⁻¹ is due to the wagging and rocking vibration transition.

4.7 Zeta Potential Analysis

The stability of rGO-Bi₂O₃ nanocomposite in the aqueous dispersion is observed by measuring the Zeta potential

distribution [38]. From Fig. 8, it is observed that the aqueous solution of rGO-Bi₂O₃ nanocomposite is found to be a negative value (-3.86 mV) of zeta potential [39]. However, the negative value of rGO-Bi₂O₃ nanocomposite is due to negative groups of stabilizing agents. Therefore, as-synthesized rGO-Bi₂O₃ nanocomposite shows the stability of nanocomposite in aqueous solution.

4.8 Cytotoxicity by MTT Assay

A549 and NCI-H460 cell lines were treated with different concentrations of the nanocomposite, and an MTT assay was performed to study the cytotoxicity of the nanocomposite. The percentage of live cells in each cell line is presented in Figs. 9 and 10. The result shows the cell viability in cancer cell lines treated with GO, rGO, and rGO-Bi₂O₃ nanocomposite at different concentrations (20–180 μg/mL). As compared to the control, the percentage of inhibition was found to be high with an increase in the concentration of nanocomposite. Cytotoxicity activity of GO against the A549 and NCI-H460 cell line the IC₅₀ values are 160 μg/mL and 150 μg/mL for 24 h of incubation (Figs. 9, 10a). Whereas, for the cytotoxicity of synthesized rGO from pomegranate peel extract against the A549 and NCI-H460 cell line the IC₅₀ values were 150 μg/mL and 120 μg/mL for 24 h of incubation (Figs. 9, 10b). The rGO-Bi₂O₃ nanocomposite has a more inhibitory effect on the cell viability with an IC₅₀ of 60 μg/mL and 80 μg/mL which is higher than GO and rGO against A549 and NCI-H460 cell lines (Figs. 9, 10c). The enhanced anti-cancer activity of rGO-Bi₂O₃ is not simply because of the additive effects of two components (rGO and Bi₂O₃). This is due to the enhancement in intercellular deliver properties of rGO sheets, the cells can accumulate more with Bi₂O₃ NP when they are conjugated to rGO sheets. Nevertheless, the results show higher cell death in the NCI-H460 cell line compared with the A549 cell line. Most

Fig. 8 Zeta potential analysis of rGO-Bi₂O₃ nanocomposite

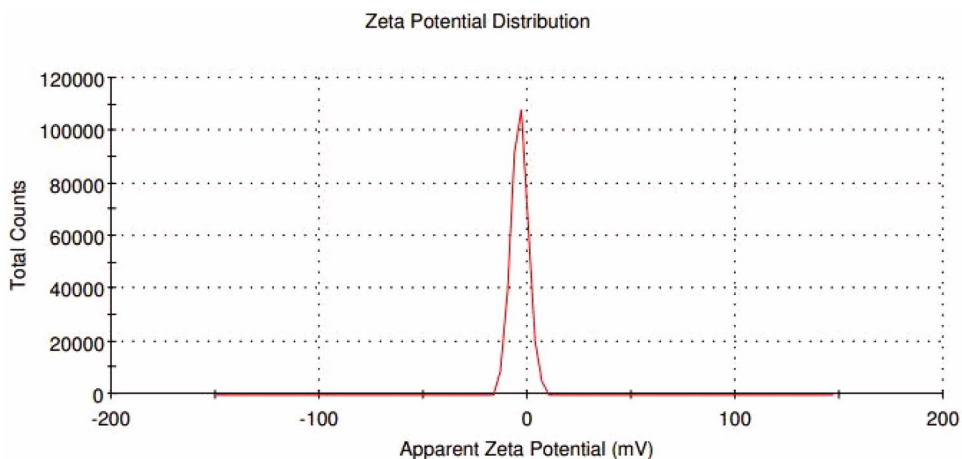


Fig. 9 MTT assay data showing survival percentage of A549 cells treated with different concentrations (20–180 $\mu\text{g/mL}$) of **a** GO, **b** rGO, and **c** rGO– Bi_2O_3 nanocomposite for 24 h. The interconnected lines indicate a significant difference between the control and treated cell lines

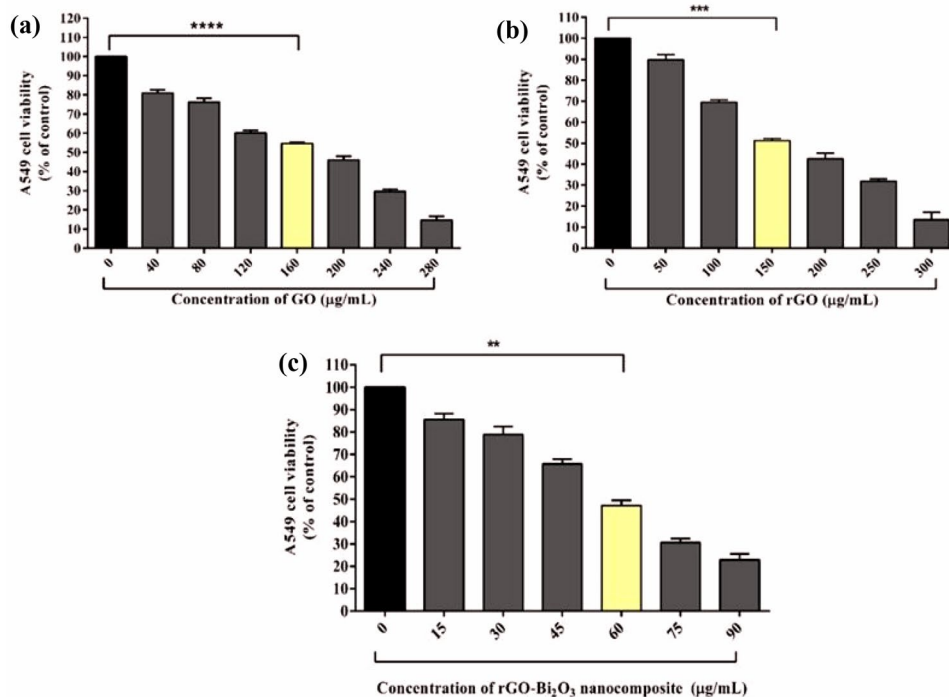
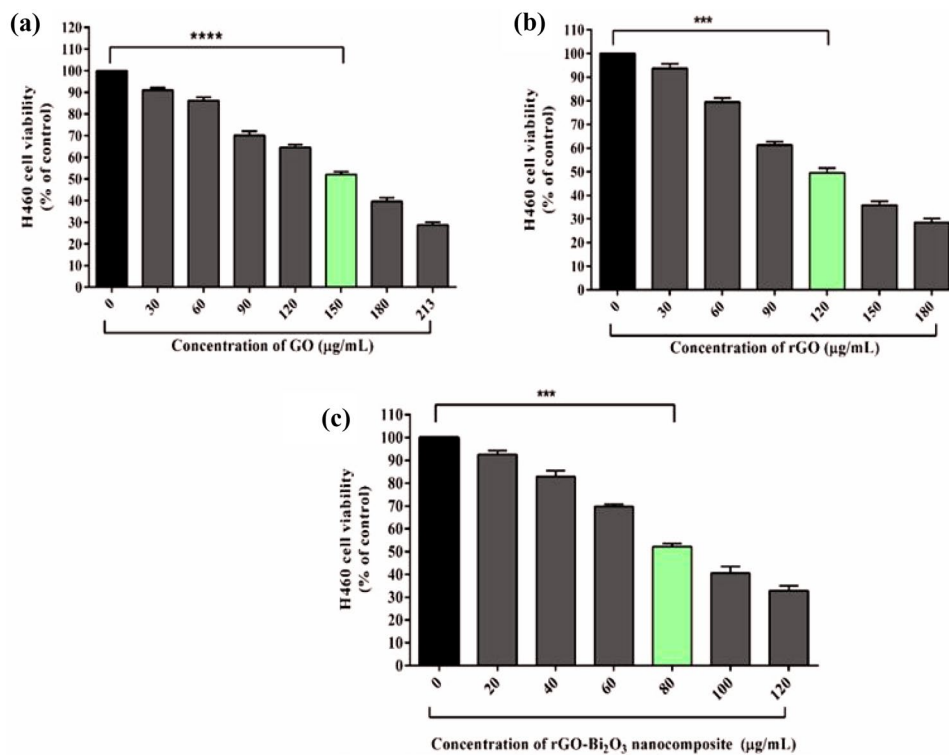


Fig. 10 MTT assay data showing survival percentage of NCI-H460 cells treated with different concentrations (20–180 $\mu\text{g/mL}$) of **a** GO, **b** rGO, and **c** rGO– Bi_2O_3 nanocomposite for 24 h. The interconnected lines indicate a significant difference between the control and treated cell lines



differences in cell death are seen after 24 h of incubation with different concentrations of nanocomposites, such that there are significantly lower molarity rates in the NCI-H460 cancer cell line compared with A549 cell lines at all

concentrations of treatment with the nanocomposite. This study demonstrates that bismuth oxide nanoparticles may stimulate ROS and its effect on intercellular components which leads to cell death.

4.9 Apoptotic Effects by AO/EtBr

The AO/EtBr staining technique was used in the present study to check the apoptotic potential of GO, rGO, and rGO–Bi₂O₃ nanocomposite. The AO/EtBr staining observation demonstrates the morphological, cellular changes, and the mechanism of cell death induced by GO, rGO, and rGO–Bi₂O₃ was due to apoptosis in cells as evident by the characteristics of nuclear changes such as cell shrinkage, nuclear fragmentation, and chromatin condensation. After 24 h of treatment with their respective IC₅₀ concentrations, samples induced apoptotic changes in the A549 and NCI-H460 lung cancer cells were observed (Fig. 11). The intact, apoptotic, and necrotic cells were monitored under the fluorescence microscope. As a result, normal intact cells (green fluorescence), early or late apoptosis (yellowish orange and reddish fluorescence), and cells with condensed chromatin and fragmented nuclei. The necrotic (orange fluorescence) will have normal morphology with no chromatin condensation. The untreated cells did not undergo any morphological changes, and the nuclei as well as cytoplasm (uniform green fluorescence). Thus, the consequence of AO/EtBr staining indicated that both A549 and NCI-H460 cells were undergoing apoptosis after GO, rGO, and rGO–Bi₂O₃ treatment. There is an increase in apoptotic cells after the treatment of rGO–Bi₂O₃ nanocomposite. The result suggested that GO, rGO, and rGO–Bi₂O₃ could induce apoptosis in both types of cells.

4.10 Intracellular ROS Measurement

Reactive oxygen species are unpaired valance shell electrons. They can damage the cells and ultimately cause

cell death. Due to various metabolic activities, a very low amount of ROS is produced in the physiological system. In general, ROS are produced from the mitochondrial respiratory chain. In the present study, superoxide is generated by using a fluorescent probe DCFH-DA. The A549 and NCI-H460 lung cancer cells were treated with GO, rGO, and rGO–Bi₂O₃ nanocomposite to determine the efficacy of ROS production by the drug to inhibit the proliferation of cancer cells. Fluorescence microscopic images reveal ROS generation in cancer cells (Fig. 12). As a consequence, this drug can be more effective for further cancer treatment.

4.11 Hoechst Staining

Apoptosis is considered a vital component of various processes in chemically-induced cell death, embryonic development, and normal cell turnover [40]. It is characterized by distinct morphological characteristics. For nuclear staining, Hoechst 33258 dyes are mainly used because they are permeable to cells, fluoresce and water-soluble. As shown in Fig. 13 the Hoechst stain was used to measure the chromatin or nuclear damage after the treatment. Consequently, this result suggests that the treatment with GO, rGO, and rGO–Bi₂O₃ nanocomposite induce nuclear damage. From the scrutiny, it was found that the Hoechst stain indicated remarkable changes from untreated cells. After 24 h of exposure to GO, rGO, and rGO–Bi₂O₃ nanocomposite, the cell showed apoptotic changes that induced apoptotic bodies, cell shrinkage, and DNA damage. The rGO–Bi₂O₃ nanocomposite acquired apoptotic features with evidence of membrane blebbing and nuclear fragmentation.

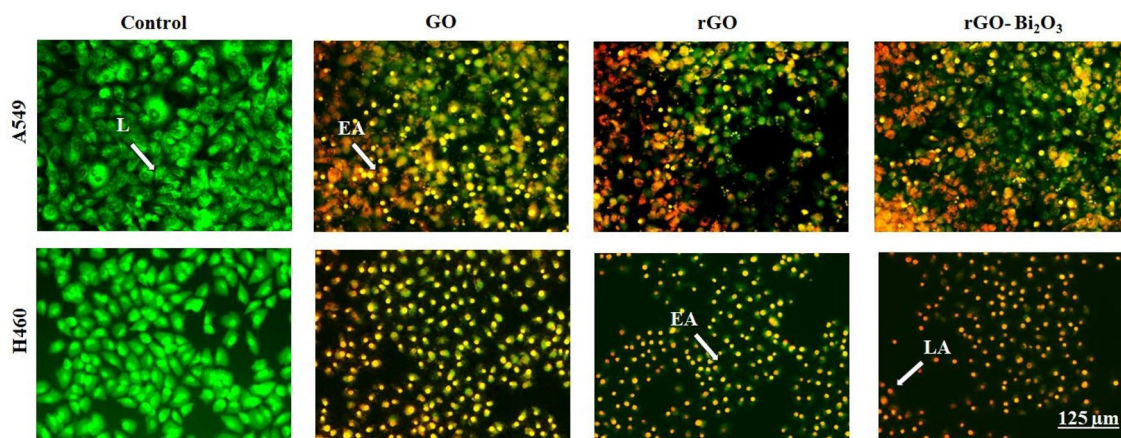


Fig. 11 Detection of apoptosis by acridine orange and ethidium bromide (AO/EtBr) staining method in A549 and NCI-H460 cells treated with GO, rGO, and rGO–Bi₂O₃ nanocomposite for 24 h. Cells stained

green are normal intact cells (L); yellowish orange colored cells are early apoptosis (EA); red-colored cells are late apoptosis (LA)

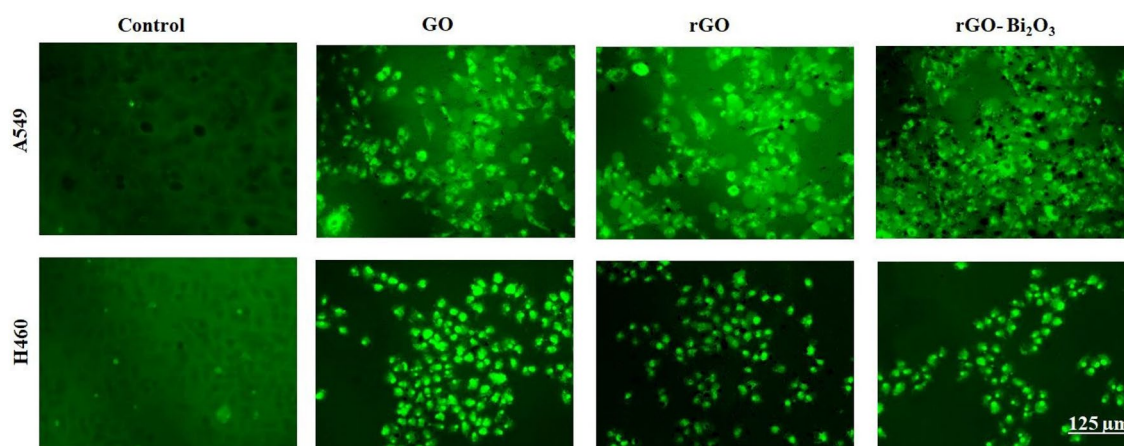


Fig. 12 Detection of apoptosis by DCFH-DA staining method in A549 and NCI-H460 cells treated with GO, rGO, and rGO–Bi₂O₃ nanocomposite for 24 h

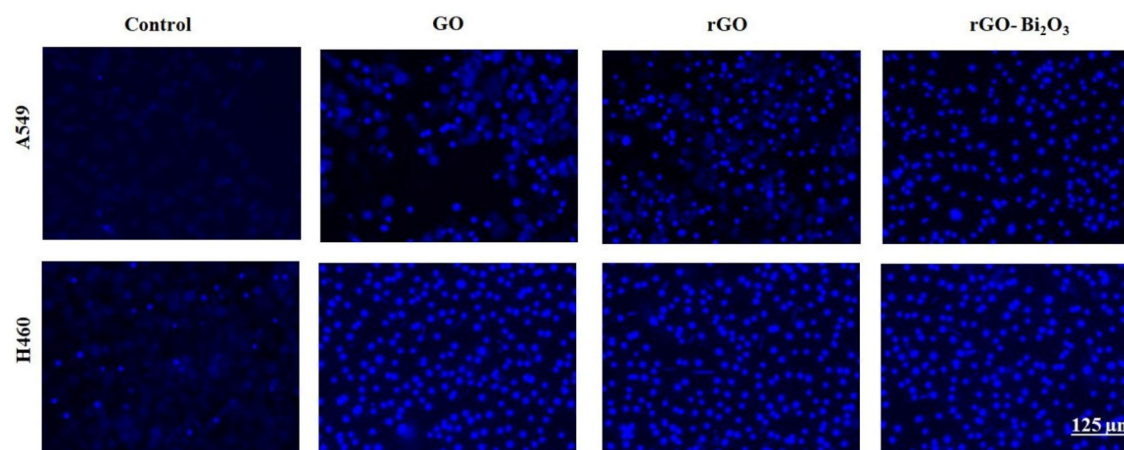


Fig. 13 Nuclear staining of A549 and NCI-H460 lung cancer cells using Hoechst 33258 staining. After 24 h of treatment, the cell line exhibits membrane blebbing, cell shrinkage, nuclear fragmentation, and DNA condensation

5 Conclusion

Graphene oxide was synthesized successfully by modified Hummer's method, and a simple and expedient method is used by using pomegranate peel extract for the reduction of graphene oxide. rGO–Bi₂O₃ nanocomposite has been synthesized by hydrothermal method. The result shows the formation of the sp² network in rGO after the reduction of GO, as confirmed by XRD. SEM image showing Bi₂O₃ nanoneedle has strongly anchored on the surface of rGO sheets. Elemental compositions and allotropes of carbon were examined using FT-Raman spectroscopy and EDAX. FTIR analysis shows that the oxygen-containing functional groups are eliminated from GO by reduction with pomegranate peel extract. Stability of the rGO–Bi₂O₃

nanocomposite were confirmed by zeta potential analysis. GO, rGO, and rGO–Bi₂O₃ nanocomposite emerged as impending anticancer agents against human lung cancer cells, namely A549 and NCI-H460. Interestingly, the cell viability was found to be reduced when an increase in the concentration of GO, rGO, and rGO–Bi₂O₃ nanocomposite. This takes place due to the stimulation of ROS by nanocomposites and by their cellular component activity which leads to cell death. Therefore, the synthesized material is proven to be a promising candidate as an anticancer agent in human lung cancer therapy.

Author contributions The corresponding author AP: Conceptualization, resource, investigation, reviews, and supervision. The first author SAA: Conceptualization, data curation, writing original draft, editing, and revision. SP and VR: Anti-cancer application analysis.

Funding The authors did not receive support from any organization for submitted work.

Declarations

Conflict of interest The author declares that there is no competing financial or personal relationship regarding the publication of this paper.

References

1. L.A. Loeb, V.L. Ernster, K.E. Warner, J. Abbotts, J. Laszlo, *Cancer Res.* **44**, 5940 (1984)
2. D. Reshmi Agnes Preethi, S. Prabhu, V. Ravikumar, A. Philominal, *Mater. Today Commun.* **33**, 104462 (2022)
3. M. Sheikhpour, M. Naghinejad, A. Kasaeia, A. Lohrasb, S.S. Shahraeini, S. Zomorodbakhsh, *Int. J. Nanomed.* **15**, 7063 (2020)
4. F. Kheiltash, K. Parivar, N. HayatiRoodbari, B. Sadeghi, A. Badieli, *Iran. J. Basic Med. Sci.* **23**, 871 (2020)
5. T. Kavinkumar, K. Varunkumar, V. Ravikumar, S. Manivannan, *J. Colloid Interface Sci.* **505**, 1125 (2017)
6. S. Marta, D. Ilona, J. Anna, S. Dariusz, *J. Nanomater.* **190**, 1 (2014)
7. X.J. Lee, B.Y.Z. Hiew, K.C. Lai, L.Y. Lee, S. Gan, G. SuchithraThangalazhy, S. Rigby, *J. Taiwan Inst. Chem. Eng.* **98**, 163 (2019)
8. S. Mikhailov (ed.), *Physics and Applications of Graphene – Theory* (IntechOpen, London, 2011), p. 475
9. M. Kocijan, L. Ćurković, I. Bdikin, G. Otero-Irurueta, M.J. Hortigüela, G. Gonçalves, T. Radošević, D. Vengust, M. Podlogar, *Appl. Sci.* **12**, 385 (2022)
10. B. Sabayan, N. Goudarzian, M.H. Moslemian, R. Mohebat, *J. Environ. Treat Techn.* **8**, 488 (2020)
11. E. Turrini, L. Ferruzzi, C. Fimognari, *Oxid. Med. Cell. Longev.* (2015). <https://doi.org/10.1155/2015/938475>
12. M.F. Abdullah, R. Zakaria, S.H.S. Zein, *RSC Adv.* **4**, 34510 (2014)
13. M. Kocijan, L. Ćurković, D. Ljubas, K. Mužina, I. Bačić, T. Radošević, M. Podlogar, I. Bdikin, G. Otero-Irurueta, M.J. Hortigüela, G. Gonçalves, *Appl. Sci.* **11**, 3966 (2021)
14. Y. Liu, X. Du, C. Wu, Y. Liu, Y. Liu, G. Zhao, *J. Mater. Sci. Mater.* **31**, 8637 (2020)
15. Y. Tian, P. Deng, Y. Wu, J. Li, J. Liu, G. Li, Q. He, *J. Electrochem. Soc.* **167**, 046514 (2020)
16. Y. Zhao, D. Zhao, C. Chen, X. Wang, *J. Colloid Interface Sci.* **405**, 211 (2013)
17. S. Nehru, S. Sakthinathan, P. Tamizhdurai, T.W. Chiu, K. Shanthi, *J. Nanosci. Nanotechnol.* **20**, 3148 (2020)
18. M. Arnaiz, C. Botas, D. Carriazo, R. Mysyk, F. Mijangos, E. Goikolea, *Electrochim. Acta.* **284**, 542–550 (2018)
19. M.S. Selim, N.A. Samak, Z. Hao, J. Xing, *Mater. Chem. Phys.* **239**, 122300 (2020)
20. M. Ahamed, M.J. Akhtar, M.A.M. Khan, H.A. Alhadlaq, *Polymers* **13**, 3350 (2021)
21. T.R. Das, S. Patra, R. Madhuri, P.K. Sharma, *J. Colloid Interface Sci.* **509**, 82 (2018)
22. R. Hernandez-Delgadillo, C.M. García-Cuellar, Y. Sánchez-Pérez, N. Pineda-Aguilar, M.A. Martínez-Martínez, E.E. Rangel-Padilla, C. Cabral-Romero, *Int. J. Nanomed.* **13**, 6089 (2018)
23. Y. Liao, W. Wang, X. Huang, Y. Sun, S. Tian, P. Cai, *Sci. Rep.* **8**, 15188 (2018)
24. A. Martin, A. Sarkar, *Nanotoxicology* **11**, 713 (2017)
25. D. Maruthamani, S. Vadivel, M. Kumaravel, B. Saravanakuma, B. Paul, S.S. Dhar, A. Habibi-Yangjeh, A. Manikandan, G. Ramadoss, *J. Colloid Interface Sci.* **15**, 449 (2017)
26. P.C. Nethravathi, M.V. Manjula, S. Devaraja, M. Sakar, D. Suresh, *J. Photochem. Photobiol. A: Chem.* **435**, 114295 (2023)
27. M. Long, D. Li, H. Li, L. Wang, Q. Zhao, Q. Wen, F. Song, *Phys. Chem. Chem. Phys.* (2022). <https://doi.org/10.1039/D2CP04434J>
28. W.D. Yang, Y.J. Lin, *Int. J. Electrochem. Sci.* **15**, 1915 (2020)
29. K. Lakshmanamoorthy, S. Prabhu, V. Ravikumar, S. Manivannan, *J. Inorg. Organomet. Polym. Mater.* **32**, 3417 (2022)
30. M. Ahamed, M.J. Akhtar, M.A.M. Khan, Z.M. Alaizeri, H.A. Alhadlaq, *Nanomaterials (Basel)* **9**, 1709 (2019)
31. A. Neha, A. Aditya, K.S. Vasu, A.K. Sood, *Nanoscale* (2013). <https://doi.org/10.1039/C3NR33190C>
32. X.J. Lee, H.N. Lim, N.S.K. Gowthaman, M.B.A. Rahman, C.A.C. Abdullah, M. Kasturi, *Appl. Surf. Sci.* **512**, 145738 (2020)
33. D. Kichukova, I. Spassova, A. Kostadinova, A. Staneva, D. Kovacheva, *Nanomaterials (Basel)* **12**, 2096 (2022)
34. P. Phukan, R. Narzary, P.P. Sahu, *Mater. Sci. Semicond. Process.* **104**, 104670 (2019)
35. M. Yadav, S. Chatterji, S.K. Gupta, G. Watal, *Int. J. Pharm. Sci.* **6**, 539 (2014)
36. T. Kuila, S. Bose, P. Khanra, A.K. Mishra, N.H. Kim, J.H. Lee, *Carbon* **50**, 914 (2012)
37. H. Liang, X. Liu, D. Gao, Y. Li, *Nano Res.* **10**, 3690 (2017)
38. W. Gu, H. Li, X. Niu, J. Zhou, *Green Process. Synth.* **11**, 316 (2022)
39. D. Li, M.B. Muller, S. Gilje, S.R.B. Kaner, G.G. Wallace, *Nat. Nanotechnol.* **3**, 101 (2008)
40. E.M. Ngigi, B.P. George, H. Abrahamse, P.N. Nomngongo, J.C. Ngila, *J. Nanopart. Res.* **22**, 195 (2020)

Publisher's Note Springer Nature remains neutral with regard to jurisdictional claims in published maps and institutional affiliations.

Springer Nature or its licensor (e.g. a society or other partner) holds exclusive rights to this article under a publishing agreement with the author(s) or other rightsholder(s); author self-archiving of the accepted manuscript version of this article is solely governed by the terms of such publishing agreement and applicable law.